

# Adsorption of ammonium on biochar prepared from giant reed

Jie Hou<sup>1,2</sup> · Lei Huang<sup>1,2</sup> · Zhimin Yang<sup>1,2</sup> · Yaqi Zhao<sup>1,2</sup> · Chaoren Deng<sup>1</sup> · Yucheng Chen<sup>1,2</sup> · Xin Li<sup>1</sup>

Received: 26 January 2016 / Accepted: 13 June 2016 / Published online: 25 June 2016  
© Springer-Verlag Berlin Heidelberg 2016

**Abstract** Giant reed was used as precursor for making biochar in order for the adsorption of  $\text{NH}_4^+\text{-N}$  from aqueous solution. And the adsorption of the product to  $\text{NH}_4^+\text{-N}$  was examined. The surface features of biochar were investigated by Fourier transform infrared spectroscopy (FTIR), scanning electron microscopy/energy dispersive spectrometer (SEM-EDS), and X-ray diffraction (XRD). XRD patterns showed several peaks and correspond to the high amount of crystalline material. The crystals contain KCl,  $\text{K}_2\text{O}$ , CaO, MgO, and SiO and possess high surface area which enhances adsorption. The influence of different parameters such as initial concentration, adsorption time, pH, and ionic strength has been carried out. The adsorption could reach equilibrium through 24 h reaction and had the best adsorption amount at the solution pH values from 7 to 9. The cation has great influence on the adsorption of  $\text{NH}_4^+\text{-N}$ , whereas the anion exerted a weaker effect. The adsorption followed pseudo-first-order and pseudo-second-order models. And the intraparticle diffusion and desorption studies further elucidated that the mechanism of adsorption on the product was ion exchange. The product equilibrium data

was well described by the Langmuir and Freundlich model. The maximum adsorption capacities were 1.490 mg/g. Biochar derived from giant reed at 500 °C was suggested as a promising adsorbent for the removal of  $\text{NH}_4^+\text{-N}$  from slightly polluted wastewater.

**Keywords** Biochar · Giant reed · Ammonium · Adsorption experiments · Adsorption kinetics and isotherms

## Introduction

Nitrogen compounds as a basic block of plant and animal proteins are nutrients essential to all forms of living life. However, it can become toxic depending on the concentration. For example, ammonia is toxic to fish and other forms of aquatic life in very low concentration, about 0.2 mg/L (Haralambous et al. 1992), and high concentration of them in ground and surface waters can lead to increase of oxygen demand and eutrophication, an intense accumulation of algae. Physical, chemical, and biological purification methods have been used in wastewater treatment for minimizing the concentration of ammonium ions. Among these methods, adsorption using biochar has been widely considered.

Biochar is the carbon-rich solid product from organic matters, and it is generally created for safe and potentially beneficial storage in soil compared with other traditional solid production from thermo-chemical conversion such as charcoal, coke, and activated carbon (Wang et al, 2015). Most studies have shown that biochar application to soil will improve soil environment, enhance soil fertility, and can effectively isolate carbon, reduce greenhouse effect (Yao et al. 2011), and increases soil water storage capacity, hydraulic conductivity (both saturated and unsaturated) internal drainage, and aeration of the topsoil (Marousek 2014). Currently, biochar is used to control the fate and toxicity of organic compounds,

Responsible editor: Hailong Wang

**Electronic supplementary material** The online version of this article (doi:10.1007/s11356-016-7084-4) contains supplementary material, which is available to authorized users.

✉ Lei Huang  
panda11@126.com

<sup>1</sup> Key Laboratory of the Three Gorges Reservoir Region's Eco-Environment (Ministry of Education), College of Resource and Environment, Southwest University, 216 Tiansheng St, Chongqing 400715, People's Republic of China

<sup>2</sup> Chongqing Key Laboratory of Agricultural Resources and Environment, Chongqing 400716, People's Republic of China

including hydrophobic organic compounds (Zhou et al. 2010), pesticides (Uchimiya et al. 2012), and antibiotics (Liu et al. 2012), because of the strong sorption affinities for various contaminants and low cost of the material.

The ability of biochar to adsorb contaminants depends on physicochemical characteristics, which vary greatly with the raw materials and pyrolysis conditions (Sun et al. 2011). Biochar with extensively porous structures and high surface area are generally prepared from raw materials pyrolyzed at high temperatures (400 to 700 °C) and exhibit a considerable adsorption capacity (Liang et al. 2008). It is well known that  $\text{NH}_4^+$  adsorption was probably related to acidic function groups on the biochar, such as, phenolic-OH and carboxyl C=O (Wang et al. 2015). Whereas,  $\text{NO}_3^-$  sorption at the biochar surface may be mainly due to electrostatic interaction (outer-sphere complexation mechanism) and to a lesser extent ionic exchange mechanism (Chintala et al. 2015).

Biomass feedstock, heating rate, heat treatment temperature, and holding time are known to exert significant effects on the structural and chemical characteristics of the produced biochar (Lin et al. 2012). Raw materials with high lignin content can obtain higher biochar yield, which also needs appropriate pyrolysis temperature (e.g., 500 °C) (Demirbas 2006; Fushimi et al. 2003). During pyrolysis, cellulose and lignin liquefaction will reduce tar yield; however, given that the lignin and cellulose chain reaction generates lipid groups (Worasuwannarak et al. 2007), biochar output will be increased. The heating rate will also significantly affect biochar yield, for which a low heating rate is favorable. Biochar at low temperature may possess several unique properties (e.g., cation-exchange capacity), and the performance will improve nutrient uptake and enhance crop yield (Day et al. 2005). Biochar obtained at high-temperature conditions will possess higher absorption capacity (Ogawa et al. 2006) and may reduce the influence of toxic substances on plant growth. The surface of biochar contains a large number of acid groups, which are obtained at a lower temperature. These groups are not conducive to microbial attachment, until the surface is oxidized to achieve higher water holding capacity (Joseph et al. 2010).

At present, there have been adsorbents prepared from biological residues (Marousek 2014). And new research showed that the biochar can be produced by the waste and waste heat in order to reduce the cost of biochar (Marousek 2014). In China, giant reed has been widely used in constructed wetlands for wastewater treatment, but most of them are burned on the spot after harvest which leads to air pollution. The resulting emission of volatile organic compound, carbon monoxide, and carbon dioxide ( $\text{CO}_2$ ) can account for 0.64 to 0.94 % of the country's total emissions. An alternative to destroying harvested biomass is putting them to beneficial use, especially in the context of a developing country (Huang et al. 2015). In this study, we used giant reed to produce biological carbon materials at 500 °C (AD-500)

and focuses on (a) determining the surface characteristics of AD-500 properties, (b) understanding the effects of pH, effluent concentration, temperature, and adsorption time on the  $\text{NH}_4^+$ -N removal efficiency from aqueous solutions, and (c) evaluating the process kinetics and thermodynamics of  $\text{NH}_4^+$ -N adsorption on biochar derived from giant reed.

## Materials and methods

### Materials

Giant reed straw used in this study was obtained from a constructed wetland treating wastewater in Gaofeng, Chongqing, China. The straw was washed with tap water to remove dirt and air-dried at room temperature for 2 to 3 days. The sample was then dried at 100 °C for 48 h in an oven and eventually placed in a desiccator (Huang et al. 2015). The determination method of lignocellulose components in giant reed provided by Ma et al. (2009), and the final results as follows: cellulose  $43.17 \pm 0.8$  wt.%<sub>db</sub>, hemicellulose  $28.97 \pm 0.2$  wt.%<sub>db</sub>, lignin  $15 \pm 0.3$  wt.%<sub>db</sub>, and ash content  $0.27 \pm 0.01$  wt.%<sub>db</sub>.

Biochar was obtained as follows: giant reed straw was carbonized at 500 °C for 2 h in the furnace (SMX1100-20, Shanghai Shangqun Electronic Science and Technology Co., Ltd, China) under high purity  $\text{N}_2$  (99.999 %) flow at 50 mL/min, and at a heating rate of 10 °C/min. After being cooled under an ambient temperature, the sample was bottled. The obtained biochar were then crushed and sieved to a desired particle size (18–40 mesh) using heavy-duty cutting mill (FW-80, Shanghai Hu Yue Ming Scientific Instrument Co., Ltd, China). Finally, the samples were washed with distilled water until the pH level was stabilized and dried in a vacuum oven at 80 °C for 24 h and then stored in a tightly closed screw cap bottle.

### Test method

#### Adsorption experiments

Adsorption experiments were performed by shaking 0.5 g of AD-500 with a certain concentration of  $\text{NH}_4^+$ -N solution in an oscillator (ZHWHY-2102C, Shanghai Bozhen Instrument Equipment Factory, China) at a solid-liquid ratio of 1:20. Continuous mixing was provided during the experiment, and the oscillator was used to control the desired temperature (25 °C) and shaking rate (150 rpm). And the initial pH levels of the experimental solutions were adjusted to  $7.0 \pm 0.1$  by the addition of HCl or NaOH solutions. Finally, the supernatant liquids were filtered through 0.42  $\mu\text{m}$  cellulose acetate membrane and the  $\text{NH}_4^+$ -N concentration was determined by standard method.

The effects of solution pH, initial concentration, contact time, temperature, and ionic strength were investigated. The effect of initial concentration on adsorption was investigated at fixed amount of adsorption and various concentrations (2, 4, 8 mM) of adsorbate solution. The effect of pH on the removal of  $\text{NH}_4^+\text{-N}$  by AD-500 was studied by conducting experiments at different pH values (4–10) with initial  $\text{NH}_4^+\text{-N}$  concentration of 4 mM. The pH of the solutions was adjusted by using HCl or NaOH solutions. Subsequently, experiments were performed to study the effect of each individual cation ( $\text{K}^+$ ,  $\text{Ca}^{2+}$ ,  $\text{Na}^+$ , and  $\text{Mg}^{2+}$ ) present in the  $\text{NH}_4^+$  ion solution on  $\text{NH}_4^+$  removal by AD-500. Solutions with an  $\text{NH}_4^+$  ion concentration of 4 mM and individual cation concentrations in the range of 1–10 meq/L were used. KCl,  $\text{CaCl}_2$ , NaCl, and  $\text{MgCl}_2$  of analytical grade were used to prepare these solutions. The experiments with individual anions ( $\text{Cl}^-$ ,  $\text{SO}_4^{2-}$ , and  $\text{CO}_3^{2-}$ ) present alone in the  $\text{NH}_4^+$  ion solution were carried out using solutions prepared individually with  $\text{NH}_4\text{Cl}$ ,  $(\text{NH}_4)_2\text{SO}_4$ , and  $(\text{NH}_4)_2\text{CO}_3$  of analytical grade, with  $\text{NH}_4^+$  ion concentrations varying in the range of 2–25 meq/L (Huang et al. 2010). The temperature effect was assessed by equilibrating 0.5 g AD-500 with  $\text{NH}_4^+\text{-N}$  initial concentration intervals of 30, 40, 50, 60, 70, and 80 mg/L in an oscillator at 10, 25, and 40 °C for 24 h.

*The desorption experiment*

AD-500 at 0.5 g was contacted with a  $\text{NH}_4^+\text{-N}$  concentration of 4 mM until equilibrium was achieved, and the adsorption capacity of  $W_0$  (mg/g) was calculated. Then, the solid was washed with deionized water to remove any unadsorbed  $\text{NH}_4^+\text{-N}$  and dried in an oven at 60 °C. KCl, HAc-NaAc, NaOH, and alkaline potassium persulfate solution extract, were continuously used; ammonium ion concentration was determined to obtain the ion-exchange nitrogen (IEF-N), weak acid leaching of nitrogen (WAEF-N), alkali transferable nitrogen (SAEF-N), and strong oxidant transferable nitrogen (SOEF-N), respectively.

The precipitation  $W_i$  (mg/g) of various forms of nitrogen in solution was calculated, and the percentage of desorption was calculated using the following equation:

$$\text{Desorption (\%)} = \frac{W_i}{W_0} \times 100 \% \quad (i = 1, 2, 3, 4) \tag{1}$$

**Analysis method**

*Biological carbon adsorption*

The adsorption capacity  $q_e$  (mg/g) of AD to  $\text{NH}_4^+\text{-N}$  at equilibrium was calculated as follows:

$$q_e = \frac{(C_0 - C_e)V}{W} \tag{2}$$

where  $C_0$  and  $C_e$  (mg/L) are the initial and equilibrium concentrations of  $\text{NH}_4^+\text{-N}$ , respectively;  $V$  is the volume (L) of the  $\text{NH}_4^+\text{-N}$  solution, and  $W$  is the weight of the AD-500.

*Dynamic characteristics*

In order to evaluate the adsorption kinetics of  $\text{NH}_4^+\text{-N}$ , and find the appropriate adsorption dynamic model for the process, three kinds of kinetic models were applied in this study: (1) the pseudo-first-order, (2) pseudo-second-order, and (3) Elovich models.

The pseudo-first-order model is expressed as follows:

$$\log(q_e - q_t) = \log q_e - \frac{k_1}{2.303} t \tag{3}$$

Where  $q_e$  and  $q_t$  are the amounts of  $\text{NH}_4^+\text{-N}$  adsorbed (mg/g) at equilibrium time and at time  $t$ , respectively, and  $k_1$  (1/min) is the rate constant. The values of  $q_e$  and  $k_1$  were calculated from the slopes and intercepts of the plots of  $\log(q_e - q_t)$  versus  $t$ .

The pseudo-second-order model is expressed as follows:

$$\frac{t}{q_t} = \frac{1}{k_2 q_e^2} + \frac{1}{q_e} t$$

Among these quantities,

$$h = k_2 q_e^2 \tag{4}$$

where  $h$  represents the initial adsorption rate (mg/g min), and  $k_2$  (g/mg min) is the pseudo-second-order rate constant. The values of  $q_e$ ,  $k$ , and  $h$  can be obtained from the slopes and intercepts of the  $t/q_t$  versus  $t$  plots.

The Elovich model is one of the most appropriate models for describing chemisorption. The model is given as:

$$q_t = \left(\frac{1}{b}\right) \ln(ab) + \frac{1}{b} \ln t \tag{5}$$

where  $a$  is the initial adsorption rate ( $\text{mg g}^{-1} \text{min}^{-1}$ ), and  $b$  is the desorption constant ( $\text{mg g}^{-1}$ ), which can be obtained from the slopes and intercepts of  $q_t$  versus  $t$  plots.

*Thermodynamic characteristics*

Langmuir isotherm assumes that adsorption occurs at specific homogenous sites within the adsorbent (Wang et al. 2010). The general equation is given as follows:

$$\frac{c_e}{q_e} = \frac{1}{Q_m k} + \frac{1}{Q_m} C_e \tag{6}$$

Where  $Q_m$  is the maximum adsorption amount (mg/g);  $k$  is the Langmuir adsorption constant (L/mg). The values of  $Q_m$

and  $b$  were calculated from the slopes and intercepts of  $c_e/q_e$  versus  $C_e$  plots.

The Freundlich adsorption is employed to describe heterogeneous systems and reversible adsorption (Ozcan et al. 2009). The equation can be expressed in linear form as follows:

$$\log q_e = \log K_F + \left(\frac{1}{n}\right) \log C_e \quad (7)$$

where  $K_F$  is the Freundlich constant ((mg/g) (1/mg)<sup>1/n</sup>); and  $n$  represents the strength of adsorption. The Freundlich constants  $K_F$  and  $n$  can be obtained from the plot of  $\log q_e$  versus  $\log C_e$ .

## Results and discussion

### Characteristics of AD-500 and AD-RT

The surface characteristics of materials are extensively studied by using SEM-EDS and XRD. The SEM images of AD-500 and AD-RT are shown in Figs. S1 and S2 (Electronic supplementary material (ESM)). SEM imaging shows that AD-500 possesses smooth surfaces with irregular pore structure. These irregular pore structures provide specific surface areas. The analysis of atomic mass ratio is displayed in Table S1 (ESM). According to the spectrum result, both AD-RT and AD-500 contain C, O, and K. After carbonization, the Cl disappears and the contents of Ca and Mg were increased to 0.51 and 0.55 %.

The X-ray diffraction pattern of AD-500 powder used in this study is presented in Fig. S3. According to the obtained result by Jade 5.0, the peaks of  $\gamma$  and 002 disappear after carbonization, indicating that the structure of the fatty chain in straw has been decomposed or detached during the carbonization. And the XRD spectra of AD-500 showed several peaks, which are characteristic XRD peaks of AD-500 and correspond to the high amount of crystalline material. The crystals contain KCl, K<sub>2</sub>O, CaO, MgO, and SiO and possess high surface area which enhances adsorption (Wankasi and Dikio 2014).

Proximate analysis results and physical properties are some of the important adsorbent properties. Table S2 presents the properties of AD-500 (ESM). The surface area of AD-500 was found to be 345.92 m<sup>2</sup>/g and is higher than that of adsorbents, such as corn straws biochar (61.0 m<sup>2</sup>/g) but lower than that of hazelnut husk (1092 m<sup>2</sup>/g) (Imamoglu and Tekir 2008; Song et al. 2014). After carbonization, volatile matter decreased from 73.48 to 14.72 %, and the fixed carbon increased from 18.79 to 75.20 %. The elemental compositions of AD-500 and AD-RT are presented in Table S3 (ESM). The molar H/C ratios of AD-500 and AD-RT were 0.005 and 0.04,

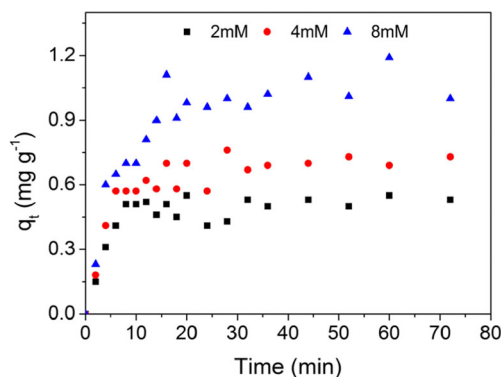


**Fig. 1** Effect of contact time and initial concentration to the adsorption to  $\text{NH}_4^+-\text{N}$

respectively, indicating high carbonization and aromaticity at 500 °C. The molar O/C ratio was also lower in AD-500 (0.12), indicating that the surface of the samples became less hydrophilic after pyrolysis. The ratios of (O+N)/C, which is a polarity index indicator, indicating increased aromaticity and decreased polarity of biochar produced at 500 °C.

The major function groups of the adsorbent are commonly identified by using FTIR spectroscopy. The infrared spectra of AD-500 are shown in Fig. S4 (ESM). The results show us that biochar possesses different functional groups. The band at around 3372 cm<sup>-1</sup> can be assigned to the -OH stretching vibration mode of hydroxyl functional groups. The vibration of hydroxyl functional groups in straw raw materials are strong and disappeared in AD-500. The peaks at 2952, 2920, and 2851 cm<sup>-1</sup> are attributed to the -CH<sub>2</sub> stretching vibration, the band intensities for aliphatic -CH<sub>2</sub> (2952 and 2851 cm<sup>-1</sup>) decrease during carbonization, indicating decreased nonpolar group content. The peaks at 1734, 1635, 1601, and 1509 cm<sup>-1</sup> represent C=O stretching of the ester bond, C=C and C=O stretching in the aromatic ring, and the C=C-C stretching vibration in the aromatic ring, respectively. In addition, the band intensities for lignin characteristic peak (1635 and 1509 cm<sup>-1</sup>) decreased significantly after carbonization, indicating lignin pyrolysis. The band at 1734 cm<sup>-1</sup> (C=O) disappears abruptly in AD-500.

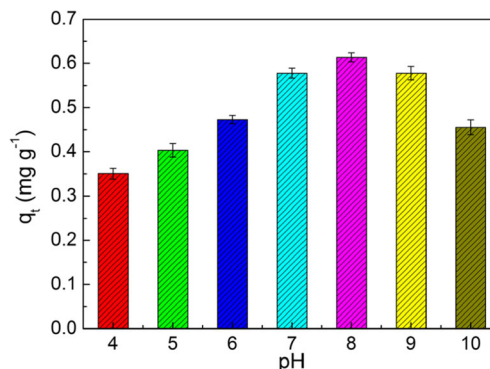
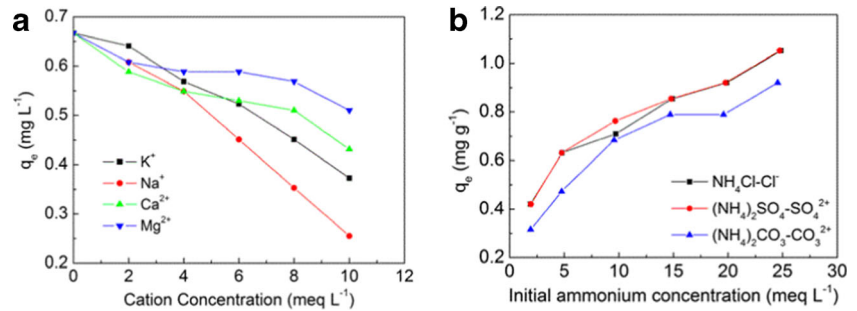


**Fig. 2** Effect of solution pH to the AD-500 adsorption to  $\text{NH}_4^+-\text{N}$

**Fig. 3** Effect of ionic strength to the AD-500 adsorption to  $\text{NH}_4^+\text{-N}$  **a** cation strength and **b** anion strength



**Influence of the initial concentration and adsorption time**

A study of the effect of contact time on the adsorption of  $\text{NH}_4^+\text{-N}$  by AD-500 at different initial concentrations was performed, and the results are depicted in Fig. 1. As shown in the figure, the adsorption rate is extremely high initially, because the  $\text{NH}_4^+\text{-N}$  is affected by the boundary-layer effect of the biochar.  $\text{NH}_4^+\text{-N}$  through its outer membrane diffusion reaches the surface and then through biochar surface adsorption and internal diffusion into the inner pore of AD-500. After 25 min, the uptake was almost constant, so 25 min could be considered the equilibrium time of  $\text{NH}_4^+\text{-N}$  adsorption. For different  $\text{NH}_4^+\text{-N}$  concentrations, the corresponding AD-500 balance adsorption increased with the increase in initial concentration level. The equilibrium adsorption amounts are 0.51, 0.68, and 0.99 mg/g at the  $\text{NH}_4^+\text{-N}$  initial concentrations of 2, 4, and 8 m, respectively. This increase is due to the fact that higher  $\text{NH}_4^+\text{-N}$  concentration strengthens the driving force between adsorbate and adsorbent and improves collision probability between AD-500 and  $\text{NH}_4^+\text{-N}$ .

**Effects of solution pH**

In the process of adsorption of  $\text{NH}_4^+\text{-N}$  by AD-500, pH value exerts an important influence on adsorption effect. In addition, the experiment was conducted in the initial pH range from 4 to 10, as shown in Fig. 2. As can be seen from the graph, the adsorption capacity of AD-500 to  $\text{NH}_4^+\text{-N}$  increased from 0.35 to 0.61 mg/g with an increased pH from 4 to 8. When pH is higher than 8, the adsorption capacity of  $\text{NH}_4^+\text{-N}$  decreased with the increase in pH. At pH 10, the adsorption quantity of AD-500 reduced to 0.46 mg/g. The effect of pH value on the adsorption capacity of AD-500 may be due to several explanations, one of which is that the surface charge of AD-500 is changed by pH, because the oxygen-containing functional groups of AD-500 surface is gradually being protonated with the decreased in pH. The electrostatic attraction between  $\text{NH}_4^+\text{-N}$  and AD-500 was weakened. Second is due to the pH change in the structure of  $\text{NH}_4^+\text{-N}$ . With pH higher than 8,  $\text{NH}_4^+\text{-N}$  transforms into  $\text{NH}_3\cdot\text{H}_2\text{O}$ , which is not easy to be adsorbed by AD-500 because of the difficulty in ion

**Fig. 4** Different kinetic models for  $\text{NH}_4^+\text{-N}$  adsorption onto AD-500 at three different initial concentrations: **a** pseudo-first-order model, **b** pseudo-second-order model, and **c** Elovich model

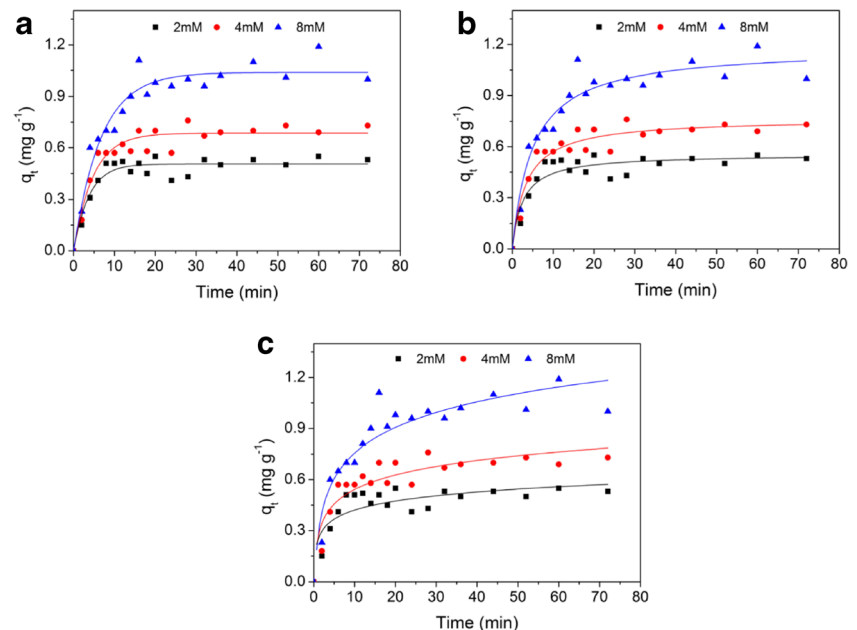


**Table 1** Kinetic parameters of the adsorption model

$C_0$ (mM)	Pseudo-first-order model			Pseudo-second-order model				Elovich model		
	$k_1$ (min <sup>-1</sup> )	$q_e$ (mg g <sup>-1</sup> )	$R^2$	$k_2$ (g mg <sup>-1</sup> min <sup>-1</sup> )	$q_e$ (mg g <sup>-1</sup> )	$h$ (g mg <sup>-1</sup> min <sup>-1</sup> )	$R^2$	$a$ (g mg <sup>-1</sup> min <sup>-1</sup> )	$b$ (mg g <sup>-1</sup> )	$R^2$
2	0.2655	0.51	0.8995	0.7126	0.55	0.2155	0.8623	1.8405	13.0246	0.7861
4	0.2098	0.69	0.9245	0.3852	0.76	0.2225	0.9234	1.0012	8.1130	0.8707
8	0.1496	1.04	0.9332	0.1716	1.17	0.2349	0.9330	0.7087	4.6131	0.8958

exchange. There is a large amount of  $H_3O^+$  in solution when pH is lower than 7. An excess  $H_3O^+$  could compete with  $NH_4^+$ , resulting in a low level of adsorbed  $NH_4^+$ . Therefore, when pH is 7–9, it is beneficial to the adsorption of  $NH_4^+$ -N by AD-500.

### Effect of ionic strength

In general, various salts exist in wastewater. The salts lead to high ionic strength which may affect the influence of  $NH_4^+$ -N adsorption on AD-500. This test for cationic  $K^+$ ,  $Na^+$ ,  $Ca^{2+}$ , and  $Mg^{2+}$ , as well as anions  $Cl^-$ ,  $SO_4^{2-}$ , and  $CO_3^{2-}$  investigated the effects of ionic strength on the properties of AD-500 adsorption of  $NH_4^+$ -N.

Figure 3 shows the effect of ionic strength on  $NH_4^+$ -N adsorption. As can be seen from Fig. 3a, the amount that AD-500 adsorbed showed a sharp decrease as the concentration of cation increased. This action indicates that the adsorption of  $NH_4^+$ -N mainly occurs by ion exchange, and the presence of various cations produce competition with  $NH_4^+$ -N. Different cations have different effects on the adsorption of  $NH_4^+$ -N. The effects of  $K^+$  and  $Na^+$  on adsorption surpassed those of  $Ca^{2+}$  and  $Mg^{2+}$  because  $K^+$  and  $Na^+$  reduce the competition with  $NH_4^+$ -N for sorption sites on AD-500, and  $Na^+$  exerts the largest inhibition effect on  $NH_4^+$ -N adsorption. Conversely, the effect of  $Mg^{2+}$  is minimal. The sequence of hindrance strength is as follows:  $Na^+ > K^+ > Ca^{2+} > Mg^{2+}$ .

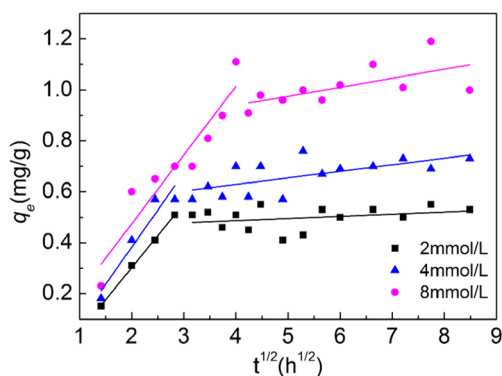
The effect of anion strength on  $NH_4^+$ -N adsorption is shown in Fig. 3b. As can be seen, the adsorption capacity

of AD-500 increases along with initial ammonium concentration, as is consistent with an early result regarding the influence of initial concentration on adsorption. Anions exert a smaller effect on  $NH_4^+$ -N adsorption performance. The effects of  $Cl^-$  and  $SO_4^{2-}$  on adsorption are the same.  $CO_3^{2-}$  relatively reduces the AD-500 adsorption of  $NH_4^+$ -N.

### Characteristics of adsorption kinetics

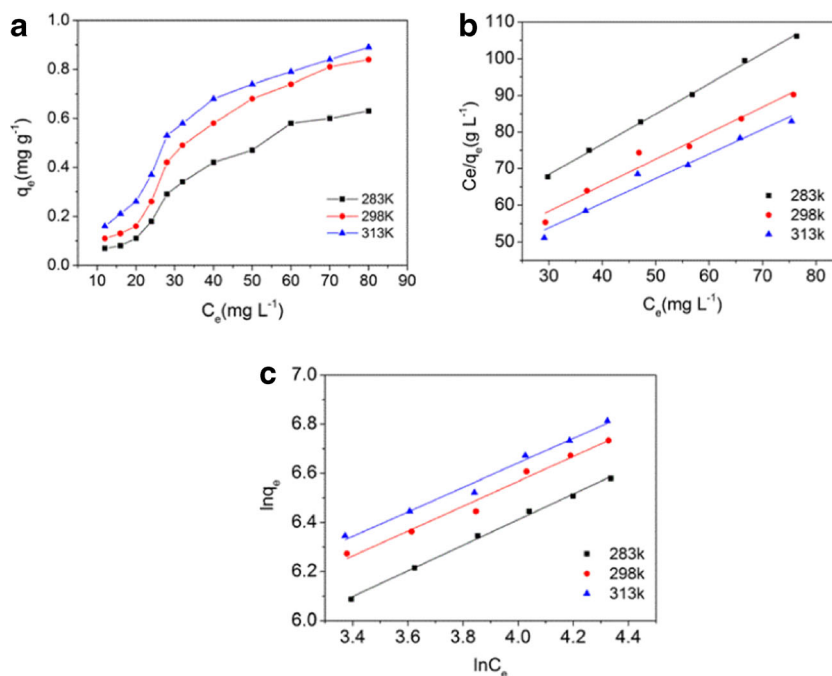
A comparison of different kinetic models for  $NH_4^+$ -N adsorption onto AD-500 is illustrated in Fig. 4, and the calculated kinetic parameters are given in Table 1.

We can observe that the correlation coefficient  $R^2$  were relatively higher for the pseudo-first-order- and pseudo-second-order models in comparison with the Elovich model, thereby indicating that the pseudo-first-order and pseudo-second-order models can describe the characteristics of  $NH_4^+$ -N adsorption by AD-500. The pseudo-first-order model describes that the adsorption rate of  $NH_4^+$ -N was influenced by the concentration of the solution, and the pseudo-second-order model described the whole process of adsorption. For the Elovich model, the obtained  $R^2$  values were relatively low, ranging from 0.7861 to 0.8958 and suggesting a nonchemical sorption mechanism. From Table 1, the values of the initial adsorption rates  $h$  increased with the increase in  $NH_4^+$ -N concentration. It can be explained by the improvement in rate of adsorption, which is attributed to the increase in solution concentration, inducing more  $NH_4^+$ -N to reach AD-500 surface in a relatively short period of time. In addition, in comparing the desorption constant  $b$  in the Elovich model, we can see that adsorption occurs more easily at a higher initial concentration of  $NH_4^+$ -N.

**Fig. 5** Intraparticle diffusion plots**Table 2** Intraparticle diffusion model constants and correlation coefficients

$C_0$ (mmol/L)	Intraparticle diffusion model					
	$Kp_1$	$Kp_2$	$C_1$	$C_2$	$R^2_1$	$R^2_2$
2	0.2520	0.00855	-0.2026	0.4528	0.9977	0.02952
4	0.2911	0.0257	-0.2000	0.5257	0.8844	0.3723
8	0.2702	0.0353	-0.066	0.7992	0.8746	0.3271

**Fig. 6** **a** Effect of temperature to the AD-500 adsorption to  $\text{NH}_4^+\text{-N}$ , **b** Langmuir isotherm for  $\text{NH}_4^+\text{-N}$  adsorption, and **c** Freundlich isotherm for  $\text{NH}_4^+\text{-N}$  adsorption



**Mechanism of adsorption**

To gain insight into the mechanisms and rate-controlling steps affecting the kinetics of adsorption, the intraparticle diffusion model has been described as:

$$q_t = k_{pi}t^{1/2} + C_i \tag{8}$$

where  $k_{pi}$  is the intra particle diffusion rate constant ( $\text{mg/g min}^{1/2}$ ), and  $C_i$  is the intercept of stage  $i$ . In other words, larger intercept, indicates the greater boundary-layer effect. To follow the intraparticle diffusion model, one plot of  $q_t$  compared with  $t^{1/2}$  should give a linear line. If the line through the origin ( $C=0$ ), indicated that the intraparticle diffusion process is the only controlling step of adsorption rate. On the other hand, if multi-linear plots are obtained then two or more steps are involved in the sorption process (Wu et al. 2005).

The amount of  $\text{NH}_4^+\text{-N}$  adsorbed compared with  $t^{1/2}$  for the intraparticle transport of  $\text{NH}_4^+\text{-N}$  by AD-500 at different initial concentrations is shown in Fig. 5. We can see from the figure that the plots presented multilinearity. The first portion which was the initial stage of adsorption is the external surface adsorption or instantaneous adsorption. In this stage, the duration is relatively

short, and the fast rising adsorption amount increased with time. The second portion was the gradual adsorption stage. In this stage, intraparticle diffusion was rate limiting.

Table 2 lists the corresponding model parameters based on the equation above. For all initial concentrations,  $k_{p1}$  was higher than  $k_{p2}$ , and  $C_2$  was larger than  $C_1$ . This finding indicates that the rate of  $\text{NH}_4^+\text{-N}$  removal was higher in the beginning because of the large surface area of the adsorbent available for the adsorption of  $\text{NH}_4^+\text{-N}$ . With the adsorption on surface of AD-500 gradually forming the boundary layer (caused by the interaction between the ion and molecular association), the capacity of adsorbent is exhausted and the uptake rate was controlled by the rate at which the adsorbate was transported from the exterior to the interior sites of adsorbent particles. None of the plots passed through the origin, revealing that intraparticle diffusion was part of the adsorption but is not the only rate-controlling step (Wang et al. 2010).

**Desorption**

Desorption experiments help in further elucidating the mechanism of adsorption. The desorption results of IEF-N, WAEF-

**Table 3** Langmuir and Freundlich constants

T (K)	Langmuir			Freundlich		
	$Q_m$ (mg/g)	$b$ (1/mg)	$R^2$	$K_F \cdot 10^3$ (mg/g (1/mg) <sup>1/n</sup> )	$1/n$	$R^2$
283	1.211	0.01894	0.9981	44.61	0.4982	0.9820
298	1.404	0.01927	0.9622	34.83	0.5063	0.9909
313	1.490	0.01990	0.9657	21.01	0.5222	0.9965

**Table 4** Lists the adsorption capacity for  $\text{NH}_4^+\text{-N}$  compared with other adsorbents

Adsorbent	Per treatments	Pyrolysis temperature ( $^{\circ}\text{C}$ )	Adsorption capacity (mg/g)	Reference
Original activated carbon	–	–	0.46	Shi et al. (2013)
Bamboo charcoal	–	600	0.85	Ding et al. (2010)
Natural Chinese clinoptilolite	–	–	11.20	Wang et al. (2006)
Oak sawdust biochar	–	300	5.31	Wang et al. (2015)
La-oak sawdust biochar	$\text{LaCl}_3$	300	10.10	Wang et al. (2015)
Rice husk-activated carbon	–	700	3.24	Zhu et al. (2012)
AD-500	–	500	1.49	This study

N, SAEF-N, and SOEF-N were found to be 28.85, 9.62, 3.85, and 11.54 %, respectively. This result indicates that various mechanisms contribute to the adsorption of  $\text{NH}_4^+\text{-N}$  on AD-500 but the ion-exchange adsorption may involve the main mechanism.

### Adsorption thermodynamic properties

The effect of temperature on the adsorption of  $\text{NH}_4^+\text{-N}$  by AD-500 is shown in Fig. 6a. As shown in the figure, the AD-500 equilibrium adsorption capacity increased sharply with the increase in temperature, indicating that adsorption of  $\text{NH}_4^+\text{-N}$  on AD-500 was an endothermic process. To further research the adsorption thermodynamic characteristics of AD-500, Langmuir and Freundlich isotherm models were fitted to the experimental data.

The adsorption isotherms of  $\text{NH}_4^+\text{-N}$  are shown in Fig. 6b, c, and the fitting parameters are listed in Table 3. As can be seen from the table, the values of  $1/n$  are between 0 and 1 at three different temperature levels, showing the existence of a high adsorption intensity.  $Q_m$  and  $b$  increased with the rise in temperature, indicating that the adsorption equilibrium capacity and adsorption rate of  $\text{NH}_4^+\text{-N}$  on AD-500 increased with an increasing temperature level. In addition, the adsorption of  $\text{NH}_4^+\text{-N}$  on AD-500 was well fitted to the Freundlich isotherm model ( $R^2=0.99$ ) and Langmuir isotherm model ( $R^2=0.96$ ). This finding indicates that in the absorption of  $\text{NH}_4^+\text{-N}$  by AD-500 with a single molecular layer and multi-molecular layer adsorption, numerous inequality and uniform surfaces are present in the biochar surface, and adsorption may involve a variety of interactive relationships between the adsorbent and the adsorbate.

Table 4 lists the adsorption capacity of different types of adsorbents for  $\text{NH}_4^+\text{-N}$ . As can be seen, the adsorption capacity of AD-500 is higher than that of original activated carbon, bamboo charcoal, but lower than that of natural Chinese clinoptilolite, oak sawdust biochar, La-oak sawdust biochar, and rice husk-activated carbon. Original activated carbon had a relatively low adsorption capacity to  $\text{NH}_4^+$  because physical adsorption was not the dominant factor compared with chemical adsorption (Shi

et al. 2013). Clinoptilolite are hydrated aluminosilicates with symmetrically stacked alumina and silica tetrahedra which results in an open and stable three-dimensional honeycomb structure with a negative charge. The negative charge within the pores is neutralized by positively charged ions (cations) such as  $\text{Na}^+$ ,  $\text{K}^+$ , and  $\text{Ca}^{2+}$ , which confers the material ion-exchange properties (Wang et al. 2006). And the adsorption of biochar to  $\text{NH}_4^+$  were potentially attributed to strong interaction. La-oak sawdust biochar presented higher  $\text{NH}_4^+$  adsorption, which may be attributed to the existing acidic function groups of phenolic-OH and carboxyl C=O (Wang et al. 2015).

### Conclusion

The AD-500 exhibits considerable potential to adsorb  $\text{NH}_4^+\text{-N}$  from aqueous solution. The AD-500 had characteristics of weak polarity and poor hydrophilicity. The present study shows that the adsorption amount was highly dependent on operating variables such as contact time, initial concentration, solution pH, ionic strength, and temperature. It is beneficial to AD-500 adsorption of  $\text{NH}_4^+\text{-N}$  when pH is 7–9, and it increased with the increase in initial concentration. The cation has great influence on the adsorption of  $\text{NH}_4^+\text{-N}$ , and the sequence of hindrance strength is as follows:  $\text{Na}^+ > \text{K}^+ > \text{Ca}^{2+} > \text{Mg}^{2+}$ . Whereas, the anion exerted a weaker effect on  $\text{NH}_4^+\text{-N}$  adsorption. The adsorption followed the pseudo-first-order and pseudo-second-order models. For the Elovich model, the obtained  $R^2$  values were relatively low, indicating a nonchemical sorption mechanism. And the intraparticle diffusion and desorption studies further elucidated that the mechanism of adsorption on the AD-500 was ion-exchange sorption. The AD-500 equilibrium data was well described by the Langmuir and Freundlich models. The maximum adsorption capacities were 1.490 mg/g. Results from this study suggested that biochar derived from giant reed at  $500^{\circ}\text{C}$  is a promising adsorbent for the removal of  $\text{NH}_4^+\text{-N}$  from slightly polluted wastewater.

**Acknowledgments** This work was supported by the National Natural Science Foundation of PR China (no. 51408493), National Science and



Technology Support Program of PR China (no. 2015BAL04B01), Research Fund for the Doctoral Program of Southwest University (no. SWU114013), and Chongqing Natural Science Foundation (NO. cstc2016jcyjA1458).

## References

- Chintala R, Mollinedo J, Schumacher TE, Papiernik SK, Malo DD, Clay DE, Kumar S, Gulbrandson DW (2015) Nitrate sorption and desorption in biochars from fast pyrolysis. *Microporous Mesoporous Mater* 179:250–257
- Day D, Evans RJ, Lee JW, Reicosky D (2005) Economical CO<sub>2</sub>, SO<sub>x</sub>, and NO<sub>x</sub> capture from fossil-fuel utilization with combined renewable hydrogen production and large-scale carbon sequestration. *Energy* 30:2558–2579
- Demirbas A (2006) Production and characterization of bio-chars from biomass via pyrolysis. *Energy Sources Part A-Recovery Utilization and Environmental Effects* 28:413–422
- Ding Y, Liu YX, Wu WX, Shi DZ, Yang M, Zhong ZK (2010) Evaluation of biochar effects on nitrogen retention and leaching in multi-layered soil columns. *Water Air Soil Pollut* 213:47–55
- Fushimi C, Araki K, Yamaguchi Y, Tsutsumi A (2003) Effect of heating rate on steam gasification of biomass. 2. Thermogravimetric-mass spectrometric (TG-MS) analysis of gas evolution. *Ind Eng Chem Res* 42:3929–3936
- Haralambous A, Maliou E, Malamis M (1992) The use of Zeolite for Ammonium uptake. *Water Science and Technology* 25:139–145
- Huang HM, Xiao XM, Yan B, Yang LP (2010) Ammonium removal from aqueous solutions by using natural Chinese (Chende) zeolite as adsorbent. *J Hazard Mater* 175:247–252
- Huang L, Chen YC, Liu G, Li SN, Liu Y, Xu G (2015) Non-isothermal pyrolysis characteristics of giant reed (*Arundo donax* L.) using thermogravimetric analysis. *Energy* 87:31–40
- Imamoglu M, Tekir O (2008) Removal of copper (II) and lead (II) ions from aqueous solutions by adsorption on activated carbon from a new precursor hazelnut husks. *Desalination* 228:108–113
- Joseph SD, Camps-Arbestain M, Lin Y, Munroe P, Chia CH, Hook J, van Zwieten L, Kimber S, Cowie A, Singh BP, Lehmann J, Foidl N, Smernik RJ, Amonette JE (2010) An investigation into the reactions of biochar in soil. *Aust J Soil Res* 48:501–515
- Liang B, Lehmann J, Solomon D, Sohi S, Thies JE, Skjemstad JO, Luizao FJ, Engelhard MH, Neves EG, Wirrick S (2008) Stability of biomass-derived black carbon in soils. *Geochimica Et Cosmochimica Acta* 72:6069–6078
- Lin Y, Munroe P, Joseph S, Henderson R, Ziolkowski A (2012) Water extractable organic carbon in untreated and chemical treated biochars. *Chemosphere* 87:151–157
- Liu P, Liu WJ, Jiang H, Chen JJ, Li WW, Yu HQ (2012) Modification of bio-char derived from fast pyrolysis of biomass and its application in removal of tetracycline from aqueous solution. *Bioresour Technol* 121:235–240
- Ma H, Liu WW, Chen X, Wu YJ, Yu ZL (2009) Enhanced enzymatic saccharification of rice straw by microwave pretreatment. *Bioresour Technol* 100:1279–1284
- Marousek J (2014a) Significant breakthrough in biochar cost reduction. *Clean Techn Environ Policy* 16:1821–1825
- Marousek J (2014b) Economically oriented process optimization in waste management. *Environ Sci Pollut Res* 21:7400–7402
- Marousek J (2014c) New concept of urban green management. *Clean Techn Environ Policy* 16:1835–1838
- Ogawa M, Okimori Y, Takahashi F (2006) Carbon sequestration by carbonization of biomass and forestation: three case studies. *Mitig Adapt Strateg Glob Chang* 11:421–436
- Ozcan AS, Gok O, Ozcan A (2009) Adsorption of lead(II) ions onto 8-hydroxy quinoline-immobilized bentonite. *J Hazard Mater* 161:499–509
- Shi M, Wang ZF, Zheng Z (2013) Effect of Na<sup>+</sup> impregnated activated carbon on the adsorption of NH<sub>4</sub><sup>+</sup>-N from aqueous solution. *J Environ Sci (China)* 25:1501–1510
- Song ZG, Lian F, Yu ZH, Zhu LY, Xing BS, Qiu WW (2014) Synthesis and characterization of a novel MnO<sub>x</sub>-loaded biochar and its adsorption properties for Cu<sup>2+</sup> in aqueous solution. *Chem Eng J* 242:36–42
- Sun K, Ro K, Guo MX, Novak J, Mashayekhi H, Xing BS (2011) Sorption of bisphenol A, 17 alpha-ethinyl estradiol and phenanthrene on thermally and hydrothermally produced biochars. *Bioresour Technol* 102:5757–5763
- Uchimiya M, Wartelle LH, Boddu VM (2012) Sorption of triazine and organophosphorus pesticides on soil and biochar. *J Agric Food Chem* 60:2989–2997
- Wang L, Zhang J, Zhao R, Li Y, Li C, Zhang CL (2010) Adsorption of Pb(II) on activated carbon prepared from *Polygonum orientale* Linn.: kinetics, isotherms, pH, and ionic strength studies. *Bioresour Technol* 101:5808–5814
- Wang YQ, Liu SJ, Xu Z, Han TW, Chuan S, Zhu T (2006) Ammonia removal from leachate solution using natural Chinese clinoptilolite. *J Hazard Mater* 136:735–740
- Wang ZH, Guo HY, Shen F, Yang G, Zhang YZ, Zeng YM, Wang LL, Xiao H, Deng SH (2015) Biochar produced from oak sawdust by lanthanum (La)-involved pyrolysis for adsorption of ammonium (NH<sub>4</sub><sup>+</sup>), nitrate (NO<sub>3</sub><sup>-</sup>), and phosphate (PO<sub>4</sub><sup>3-</sup>). *Chemosphere* 119:646–653
- Wankasi D, Dikio ED (2014) Polyvinyl chloride waste as an adsorbent for the sorption of Pb<sup>2+</sup> from aqueous solution. *J Chem*
- Worasuwannarak N, Sonobe T, Tanthapanichakoon W (2007) Pyrolysis behaviors of rice straw, rice husk, and corncob by TG-MS technique. *J Anal Appl Pyrolysis* 78:265–271
- Wu FC, Tseng RL, Juang RS (2005) Comparisons of porous and adsorption properties of carbons activated by steam and KOH. *J Colloid Interface Sci* 283:49–56
- Yao Y, Gao B, Inyang M, Zimmerman AR, Cao XD, Pullammanappallil P, Yang LY (2011) Biochar derived from anaerobically digested sugar beet tailings: characterization and phosphate removal potential. *Bioresour Technol* 102:6273–6278
- Zhou ZL, Shi DJ, Qiu YP, Sheng GD (2010) Sorptive domains of pine chars as probed by benzene and nitrobenzene. *Environ Pollut* 158:201–206
- Zhu KR, Fu H, Zhang JH, Lv XS, Tang J, Xu XH (2012) Studies on removal of NH<sub>4</sub><sup>+</sup>-N from aqueous solution by using the activated carbons derived from rice husk. *Biomass Bioenergy* 43:18–25